

**FORCED AERATION DURING HEAP LEACHING PROVIDES
INFORMATION ABOUT THE STRUCTURAL DEVELOPMENT OF POROUS
AND FRACTURED MEDIA.**

Sarat Chandra Panigrahi¹, Suryakash rout²

¹Professor, Department of Mechanical Engineering, Raajdhani Engineering College,
Bhubaneswar, Odisha

²Assistant Professor, Department of Mechanical Engineering, Raajdhani Engineering
College, Bhubaneswar, Odisha

ABSTRACT

Despite numerous methods for enhancing heap leaching performance, there are still severe limitations on industrial uses. To improve the poor permeability and leaching impact of the Yangla Copper Mine (YCM) during heap leaching, we proposed a correspondingly effective and novel method of applying forced aeration. During the column leaching experiments, the dual-media theory was used to investigate the mechanism by which forced aeration affected different types of porous and fractured media. The specimens' pores were imaged using an X-ray computed tomography (CT) set, and as the aeration rate (AR) varied, a scanning electron microscope (SEM) examined the fracture morphology of the particles within the columns.

Keywords: Yangla Copper Mine, forced aeration, X-ray

1 INTRODUCTION

A hydrometallurgical extraction method known as heap leaching is frequently used to recover rich metals from refractory or low-grade ores [1]. This method is increasingly prevalent in the mineral processing sectors due to its ease of use, cheap operating costs, high recovery rates, quick construction time, and environmental benefits [2]. The solid-liquid-gas phases that make up the leaching system interact to varying degrees depending on the system's permeability coefficient. Therefore, the permeability of the system has a significant impact on the leaching effect. However, the permeability of the ore dump is typically low because of mechanical compaction and weathering.

Researchers have suggested a variety of techniques to improve leaching performance, including loosening the waste, applying an external electric field, presenting stress waves, adding catalysts, and speeding up the growth of microorganisms [3]. Aeration assisted heap leaching is currently a relatively novel and useful leaching method used to increase leaching effectiveness. Few researchers have looked at the impact of aeration on the heap's permeability, with professionals and academics around the world focusing more on the effect of aeration in oxygen or carbon dioxide delivery. According to Brierley et al., the main difficulty impeding the growth of leaching mining is whether or not aeration should be used in heap leaching [4].

The leaching dump is a media constituted of irregular ore particles with bulks of pores and fractures. We have shown in a previous study that aeration can effectively improve the leaching effect based on MRI characterization, however, it did not involve the impact on fractures within the ore particles. Hence, during heap leaching, a concept of porous and fractured media was utilized to study the influence of aeration [5]. In this concept, two kinds of seepage channels, i.e., pore and fracture, were thought to be naturally present within the heap [6]. On one hand, the pore structure was the dominant channel for solution flow. On the other hand, fractures in ore particles were the second liquid flowing channels. Despite the relatively poor penetrability, the numerous fractures could still provide adequate storage space for the solution. Hence, a favorable environment for leaching would be obtained under the coupling effect of porous and fractured media [7, 8].

In order to clearly understand the influence of aeration rate (AR) on leaching performance, this study investigates two factors: the influence of air pumped into the novel leaching columns on the pore changes using X-ray computed tomography (CT) and the evolution of fractures within ore particles using scanning electron microscope (SEM).

Table 1
Particle size distribution of the ore.

Si ze (m m)	Cumulative weight (% by weight)	Si ze (m m)	Cumulative weight (% by weight)
0.125	0.34	4.00	70.65
0.300	1.51	5.00	87.41
0.450	3.79	6.00	91.04
1.000	7.56	7.00	95.35
2.000	30.23	8.00	97.35
3.000	50.89	9.00	100.00
0		00	

2. Experimental

The particle size distribution of the 3000 g samples, which were taken from the leaching dump of the Yangla Copper Mine (YCM) in the Chinese province of Yunnan, is shown in Table 1.

According to the particle size distribution curves typical in the field of geotechnical engineering [9], Fig. 1 shows the particle size distribution curve of the samples, the type of which belonged to A. Therefore, it may be assumed that the leaching dump of YCM contains a significant amount of loose particles, which caused the heap to be heavily compacted.

The main chemical components of the samples are shown in Fig. 2. According to analysis, the samples' average particle size was rather small [10]. Additionally, the alkaline components, such as MgO, CaO, Fe₂O₃, and Al₂O₃, whose contents were over 40%, might cause heap leaching to use a lot of acid. Therefore, utilising strategies like aeration to increase the dump's permeability may be a better strategy to boost YCM's leaching efficiency [11, 12].

Column leaching experiment

Experimental setup and leaching solution

The column leaching tests were carried out as AR varied using a unique heap leaching equipment, schematically shown in Fig. 3. Leaching columns made of plexiglass, a solid-liquid-gas circulation system, a control cabinet, and a computer made up the bulk of this device, whose maximum AR for the experiments was 0.5 m³/h. As shown in Fig. 3, raised barrels R1, R1 and R3 are also specimens S1, S1 and S3, collecting barrels T1, T2 and T3, inflating inlets U1, U2 and U3, perforated plates V1, V2 and V3, and sealing layers W1, W1 and W3. A spiral CT set (SOMATOM Sensation 16) was used for the pore imaging, and a SEM (JEOL JSM-6701F) was used to examine the fracture morphology of the samples.

Preparation

As shown in Fig. 3, the samples were well mixed according to Table 1, evenly (700 g) packed into the three columns and named S1, S2 and S3. Then, three equally-sized pebbles (the three black spots in Fig. 3) with a diameter of 2.5 mm were laid on top of the particles within the three specimens and named A, B and C. During liquid circulation, the three specimens would be saturated for 24 h.

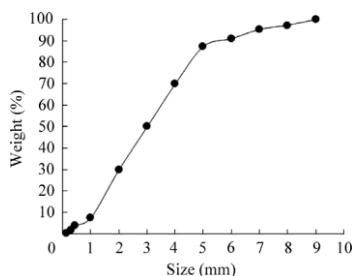


Fig. 1. Particle size distribution curve of the samples.

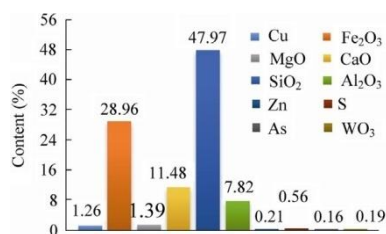


Fig. 2. Main chemical composition of the samples.

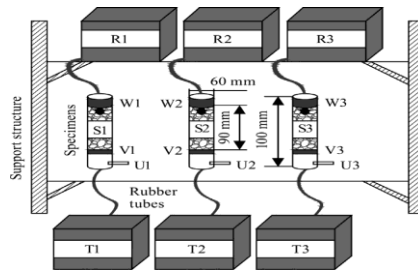


Fig. 3. Schematic of the novel column leaching apparatus.

Operation

1. Before air was pumped into the specimens, CT and SEM were separately utilized to perform the original imaging of the pore structures of S1, S2 and S3 and the fracture morphologies of A, B and C. During CT imaging, the magnification and minimum resolution cell were 4.14 and 46.9 μm respectively, and layer number of the specimens was 1500 with a thickness of 4 μm . It used a projected amplitude of 400, a rotation step of 0.9° , a tube voltage of 120 kV and a tube current of 160 μA respectively. This moment was defined to be 0 d.
2. Air was pumped into S1, S2 and S3, ARs of which were 0, 0.3 and 0.5 m^3/h respectively. Then CT and SEM were repeatedly employed to perform the images as leaching time changed (10, 20, 30 and 40 d). CT images were thresholded in Matlab to conduct the 3D reconstructions to analyze pores changes, model sizes of which were all $25.8 \text{ mm} \times 25.8 \text{ mm}$ in the x and y directions. and 80.0 mm in the z direction [16]. SEM images were imported in Image J and Fractal Fox to study the evolution of fractures.

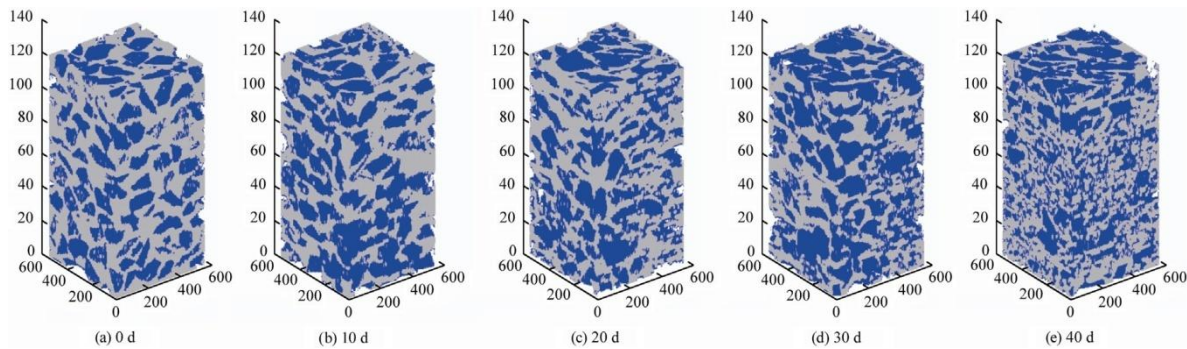


Fig. 5. 3D models of S2 as time changes.

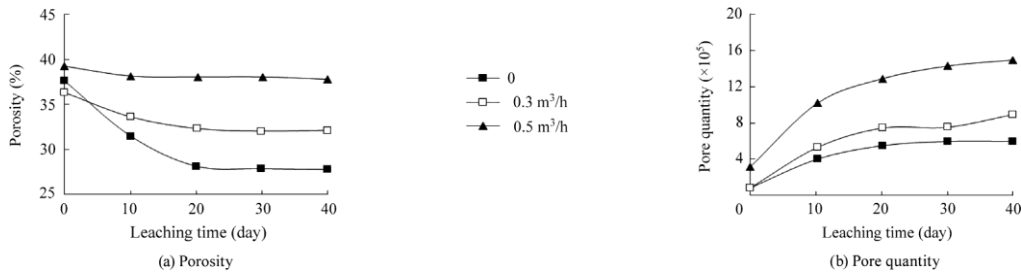


Fig. 6. Pore changes as ARs and time change.

3. RESULTS AND DISCUSSION

Pore changes

Figure 1 displays the 2D CT images and associated binary images obtained from S1, S2, and S3 as AR changes. 4 (for instance, 10 d), whose sizes were all 850 pixels in the x and y directions. The distribution of particles and pore structures showed clear differences. Particle sizes in S2 and S3 were smaller than those in S1 (Figs. 4b and e, respectively) (Fig. 4a and d).

Using S2 as an illustration, Fig. In Figure 5, which depicts the 3D reconstruction models of pore architectures as leaching time changed, the leaching solution and ore particles were represented, respectively, by blue and grey. It was evident that the ore particle sizes changed over time. The porosity of the specimens could be expressed as Eq. (1) [17].

$$V_n = \left(1 - \frac{V_a}{V}\right) \times 100\% \quad (1)$$

where n , V_a and V are the porosity, solid volume and whole volume of the models, respectively.

Within S1, S2 and S3, the porosity and pore quantity as time changes are calculated and shown in Fig. 6.

Fig. 6a shows that as AR and time change, the porosity of S1 reduces from approximately 38% to 31.8% after 10 d. However, they are relatively slow in S2 and S3. Using S3 as an example, the decline rate of porosity is only about 2%. Analytically, aeration would be substantially advantageous to the solute transport within the leaching solution, and this made the seepage paths less likely to be blocked. Therefore, porosity of the aerated system could be kept at a comparatively high level. Fig. 6b shows that the number of pores within all the three specimens all increases, however in S1, it is relatively slow, and indicates that aeration might not only shorten the leaching time but improve the reaction degree to push forward the development of the pore structure.

Evolution of fractures

As shown in Fig. 7 (e.g., 20 d), SEM images of A, B and C are acquired, then based on a specified threshold, the binary images are obtained [18,19]. There exists a small amount of fine fractures on the surface of A. However, many open fractures occurred in B and C, and fractures in the latter were wider and deeper. It indicated that aeration might increase the leaching degree by expanding the fractured structure of particles. Moreover, a higher AR was the models were effective. Based upon the binary images and results of FBDs of A and C, the evolution curves of fractures as leaching time developed were calculated, analyzed by Origin and depicted in Fig. 8. FBD of C is always higher than that of A, as shown in Fig. 8a, indicating that the amount of fractures within C is more than that in A. From Fig. 8b, it could be drawn that the fracture width of C was bigger than that of A, illustrating that aeration could effectively widen the fractures within the particles to accommodate more leaching solution, and this might improve the leaching efficiency [23].

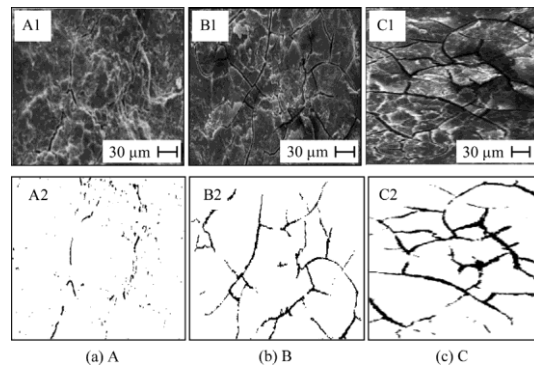


Fig. 7. SEM and its binary images of specimens (20 d).

During heap leaching, the development of fractures was a dynamic changing process which could result in a variable permeability coefficient. Thence, the seepage state within the heap was probable of being influenced. The capillary buddle model was employed to study the dynamic-permeability coefficient (DPC) and fracture ratio (DFR) of A and C, calculated by [24–27].

In this work, the fractal geometry theory was utilized to analyze the complicated fracture morphologies of A, B and C [20,21].

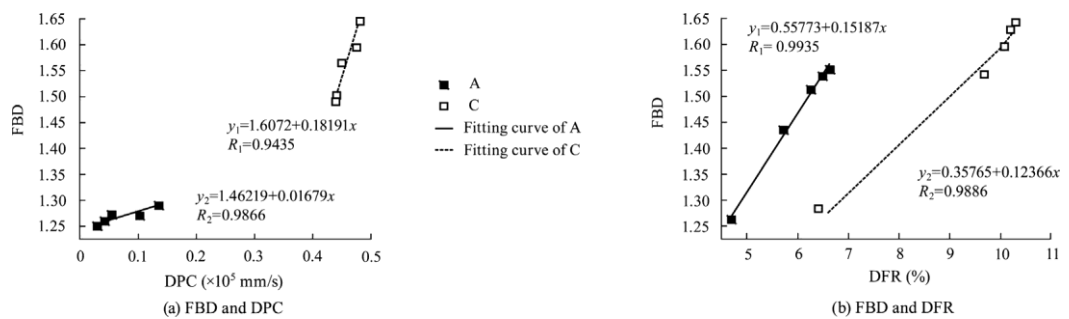


Fig. 9. The evolution curves of FBD & DPC and FBD & DFR.

Then, according to the calculation models of A and C, DPC and DFR of which are depicted in Fig. 9. From Fig. 9a, it could be seen that the average DPC of C ($0.46 \cdot 10^{-5}$)

mm/s) was obviously higher than that of A (0.09×10^{-5} mm/s). Fig. 9b shows the average DFR of C (10.2%) is higher than that of A (6.3%). It indicates that during heap leaching, the forced aeration could promote the development of fractures within ore particles. This would be beneficial in improving the permeability coefficient of the whole system to provide tremendous convenience for the solution flow.

4.CONCLUSIONS

The effects of various aeration rates (ARs) on the modifications of porous and fractured media were investigated using column leaching experiments and X-ray CT and SEM. The study found that the samples taken from the ore heap of the Yangla copper mine had a poor particle distribution. According to experimental results from a CT set, the three specimens (S1, S2, and S3 pore)'s structure changed in a number of ways when AR fluctuated. When AR increased, S2 and S3 had greater porosities (0.3 m³/h and 0.5 m³/h, respectively) and more loose and fine particles than S1 (without aeration). The studies' SEM analysis showed that the fractal box, dynamic porous, and fractured performance.

REFERENCES

1. Cariaga E, Concha F, Sepúlveda M. Flow through porous media with applications to heap leaching of copper ores. *Chem Eng J* 2005;111(2):151–65.
2. Laman JT. Solution mining and in-situ leaching. *Mining environmental handbook: effects of mining on the environment and american environmental controls on mining*; 2014.
3. Brierley JA, Brierley CL. Present and future commercial applications of biohydrometallurgy. *Hydrometallurgy* 1999;9(2–3):81–9.
4. Winterfeld PH, Wu YS. Simulation of coupled thermal-hydrological-mechanical phenomena in porous and fractured media. *Spe Journal* 2015;12 (1):369–83.
5. Song JW, Wang MY, Tang DW. Experiment on water infiltration and solute migration in porous and fractured media. *Adv Mater Res* 2014;955–959:1993–7.
6. Zhang Y, Yao F, Xu D, Ma B, Yao H. Stochastic simulation on preferential seepage channels in water-flooding reservoirs. *Electron J Geotech Eng* 2015;20 (2):803–12.
7. Nikolaevskij VN. *Mechanics of porous and fractured media*. World Scientific; 1990.
8. Tartakovsky AM, Meakin P, Scheibe TD, Wood BD. A smoothed particle hydrodynamics model for reactive transport and mineral precipitation in

- porous and fractured porous media. *Water Resour Res* 2007;43(5):5437.
9. Ai CM. Experimental and theory study on strengthening leaching of copper ores by surfactant. Beijing: University of Science and Technology Beijing;2015
 10. Winterfeld PH, Wu YS. Simulation of coupled thermal-hydrological-mechanical phenomena in porous and fractured media. *Spe Journal* 2015;12 (1):369–83.
 11. Song JW, Wang MY, Tang DW. Experiment on water infiltration and solute migration in porous and fractured media. *Adv Mater Res* 2014;955– 959:1993–7.
 12. Zhang Y, Yao F, Xu D, Ma B, Yao H. Stochastic simulation on preferential seepage channels in water-flooding reservoirs. *Electron J Geotech Eng* 2015;20 (2):803–12.
 13. Nikolaevskij VN. Mechanics of porous and fractured media. World Scientific; 1990.
 14. Tartakovsky AM, Meakin P, Scheibe TD, Wood BD. A smoothed particle hydrodynamics model for reactive transport and mineral precipitation in porous and fractured porous media. *Water Resour Res* 2007;43(5):5437.
 15. Ai CM. Experimental and theory study on strengthening leaching of copper ores by surfactant. Beijing: University of Science and Technology Beijing; 2015.
 16. Wu AX, Zhang J, Jiang HC. Improvement of porosity of low-permeability ore in heap leaching. *Min Metall Eng* 2006;26(6):5–8.
 17. Thansandote P, Harris RM, Dexter HL, Simpson Graham L, Pal Sandeep, Upton Richard J, Valko Klara. Improving the passive permeability of macrocyclic peptides: balancing permeability with other physicochemical properties. *Bioorg Med Chem* 2015;23(2):322–7.
 18. Zuo H, Wang YM, Chen XS, Jiang HC. Mechanism of improving permeability in dump by effect of electric field. *Chin J Nonferr Metals* 2007;17(3):471–5.
 19. Lizama HM. Copper bioleaching behavior in an aerated heap. *Int J Miner Process* 2001;62(1–4):257–69.
 20. Paul M, Di WR. An improved method for heap leaching of chalcopyrite. Patent: WO 2000071763 A1; 2000.
 21. Mohammadreza Fatahi, Mohammad Noaparast, Ziaeddin Shafaei Seyyed. Nickel extraction from low grade laterite by agitation leaching at atmospheric pressure. *Int J Min Sci Technol* 2014;24(4):543–8.
 22. Gardner RJ, Kiderlen M. A new algorithm for 3D reconstruction from support functions. *IEEE Trans Pattern Anal Mach Intell* 2009;31(3):556–62.
 23. Rehder B, Banh K, Neithalath N. Fracture behavior of pervious concretes: The effects of pore structure and fibers. *Eng Fract Mech* 2014;118(2):1–16.
 24. Li Y, Zeng LJ. Analyzing the grating profile parameters based on scanning-electron microscope images. *Key Eng Mater* 2008;381–382:299–300.
 25. Hs H, Chabaat M, Thimus JF. Use of scanning electron microscope and the non- local isotropic damage model to investigate fracture process zone in notched concrete beams. *Exp Mech* 2007;47(4):473–84.

26. Zhou Z, Su Y, Wang W, Yan Y. Application of the fractal geometry theory on fracture network simulation. *J Pet Explor Prod Technol* 2016;1–10.
27. Sheng JL, Wu YL. Study on the distribution characteristics of the structural planes in rock mass based on the fractal geometry theory. *Metal Mine* 2002;11 (2):231–5.
28. Ai T, Zhang R, Zhou HW, Pei JL. Box-counting methods to directly estimate the fractal dimension of a rock surface. *Appl Surf Sci* 2014;314(10):610–21.
29. Lagno Sanchez FA, Acuña GMG. Process for recovery of technical grade molybdenum from diluted leaching acid solutions (PLS), with highly concentrated arsenic, from metallurgical residues. US patent: US9279168; 2016.
30. Ju XD, Feng WJ, Zhang YJ, Zou ZS. A capillary bundle model based on aperture's exponential distribution and its application in porous media's mono direct percolation. *Adv Mater Res* 2012;594–597:2481–5.
31. Xu J, Wang Z, Ren J, Yuan J. Experimental research on permeability of undisturbed loess during the freeze-thaw process. *J Hydraul Eng* 2016;47 (9):1208–17.
32. Ghashghaei HT, Hassani A. Investigating the relationship between porosity and permeability coefficient for pervious concrete pavement by statistical modelling. *Mater Sci Appl* 2016;07(2):101–7.
33. Yu BY, Chen ZQ, Ding QL, Wang LZ. Non-Darcy flow seepage characteristics of saturated broken rocks under compression with lateral constraint. *Int J Min Sci Technol* 2016;26(6):1145–51.